Visualization of the Mammoth Hydrothermal System, Yellowstone National Park Headquarters and the Controlled Groundwater Area of the Montana Compact

Final Report for CESU USURM-90 J1580100509 from 2010 to 2012

By

Christopher M. U. Neale, Ph.D.
Professor and Director of the Remote Sensing Services Laboratory
Civil and Environmental Engineering Department
Utah State University
Logan, UT 84322-4105

Robert T. Pack, Ph.D., P.E
LASSI Service Center
Utah State University
Logan, UT 84322-4110

Saravanan Sivarajan, Ph.D.
Post-doctoral Scholar
Civil and Environmental Engineering Department
Utah State University
Logan, UT 84322-4110

Ashish Masih
Post-graduate Researcher
Civil and Environmental Engineering Department
Utah State University
Logan, UT 84322-4110

Submitted to
YNP Geology Program
Yellowstone National Park

February 28, 2013

INTRODUCTION

The National Park Service has been tasked with the monitoring of hydrothermal areas including hot springs and pools as well as other hydrothermal features within Yellowstone National Park. This monitoring has been carried out over the years using different technologies and field verification. Due to the sometimes fairly rapid change in the extent and temperature of some of these springs and hydrothermal features, a cost effective, rapid, and accurate method is necessary for the monitoring of hydrothermal areas.

Remote sensing in the thermal infrared part of the spectrum has been used in many applications to estimate surface temperature and has the advantage of obtaining a spatial representation of the temperatures as well as the extent and distribution of the hydrothermal features and the hydrothermal system. Presently, several satellite sensors such as the LANDSAT Thematic Mapper and the ASTER and MODIS instruments of the Earth Observation System platforms provide thermal infrared imagery. Unfortunately satellite thermal infrared imagery has low spatial resolution (60 to 120 meter pixels for LANDSAT and ASTER; 1000 meters for MODIS) and though the imagery covers a large surface area, it is usually collected during daytime hours and is not adequate for identifying and measuring the temperature of small hydrothermal pools and springs at high-spatial resolution in Yellowstone Park.

Airborne thermal infrared remote sensing is a proven method of obtaining high-spatial resolution thermal infrared imagery. Several applications using thermal infrared imagery can be found in the literature. For example, Torgesen et al, 2001, used airborne thermal infrared remote sensing to assess water temperatures in rivers and streams, related to fisheries habitat. Quattrochi and Luvall (2003) presented several applications using airborne and satellite based thermal infrared applications to retrieve surface parameters and processes.

The Utah State University airborne multispectral digital system includes a precision thermal infrared imager that has been used in numerous applications that require high-resolution data. Chavez et al, (2005) used thermal infrared imagery with 6-meter pixel resolution to map the spatially distributed energy balance terms (net radiation, soil heat flux, sensible heat flux and latent heat flux) and compared it with ground measured fluxes using eddy covariance flux towers and footprint functions.

Geothermal monitoring flights obtained airborne thermal, LiDAR, and visible imagery over the Park Headquarters in Mammoth and a portion of the controlled groundwater area of the Montana Compact (near the LaDuke Springs). Hydrothermal water from the Mammoth hydrothermal system flows on the travertine terraces, into the Gardner River and eventually towards the Yellowstone River north of the Park Headquarters. The image acquisition flights occurred September 23 and 24, 2010, and September 8 and 9, 2011

METHODS

Description of the Airborne Remote Sensing System

The USU airborne multispectral digital system was originally developed in 1992, based around video cameras and an Inframetrics 760 thermal infrared scanner. A description of the original system and its calibration was conducted by Neale and Crowther (1994). The system was upgraded over the years, first to include a computer on board the aircraft grabbing the images as they were collected and later the cameras were upgraded to digital cameras in 1997 as that technology matured and became commercially available.

The present generation of the USU airborne multispectral digital system is based around three Kodak Megaplus 4.2i Digital Cameras with the imaging sensor producing digital images with approximately 2000 x 2000 pixels (Cai and Neale, 1999). The camera can be operated in 8 bits or 10 bits, but for most applications images with 8 bits (256 grey scale levels) are sufficient. The shortwave spectral bands are obtained with interference filters centered in the green (0.545-0.560 ·m), red (0.665-0.680 ·m) and NIR (0.795-0.809 ·m) portions of the electro-magnetic spectrum. The cameras are mounted in a high-grade aluminum/carbon composite mount installed through a porthole in the belly of a Cessna TP206 single engine aircraft, dedicated to remote sensing. A FLIR SC640 thermal infrared camera is used to acquire thermal images in the $8 - 12$ μm range. This instrument is mounted through a different porthole aligned with the multispectral system cameras. Both the digital and thermal infrared cameras are controlled by boards and software installed in a fast PC computer with two 500 GB hard drives for storage of the imagery. Details of the multispectral system and thermal infrared camera installed in the Cessna TP206 aircraft can be seen in Figure 1.

In 2010 and 2011, the USU research aircraft was a single engine Cessna TP206A Skywagon remote sensing aircraft, N4630F.
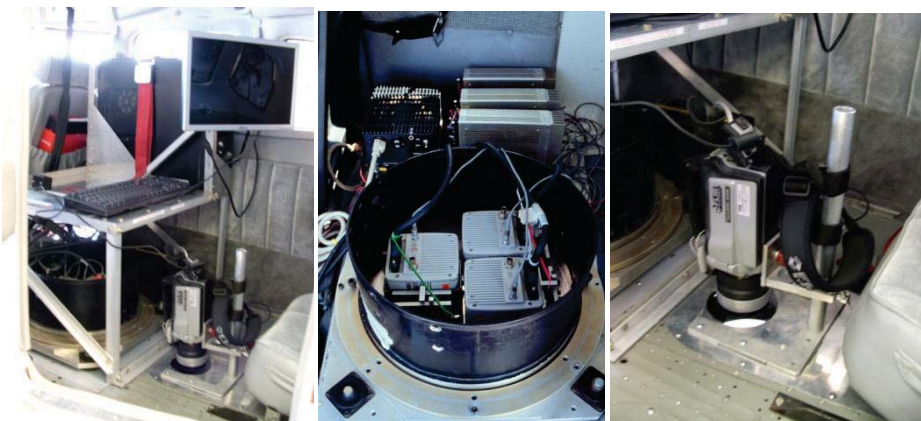
Figure 1. Details of the USU airborne multispectral remote sensing system and FLIR SC640 thermal IR camera installed in the Cessna TP206 remote sensing aircraft.

Image Acquisition

High-resolution shortwave (3 bands) and thermal infrared imagery were acquired with the USU airborne digital system over Mammoth Hot Springs, Yellowstone National Park, extending approximately 9 miles north to LaDuke Hot Springs, Montana. The pixel resolution in the shortwave bands (green, red and near-infrared) and thermal IR was 1-meter. For a 1-meter pixel resolution using the 20 mm Nikon lens of the shortwave digital cameras, the flight altitude was 6000 feet above ground level (agl). Considering the ground elevations at Yellowstone over the thermal feature sites varied between 6000 and 7500 feet, the flight altitude usually varied between 12000 and 13500 feet.

Flight lines were planned to ensure 30% overlap between images in parallel flight lines and 80% overlap along the flight lines to guarantee complete coverage over the study areas and a flight altitude to capture the appropriate resolution at an average ground altitude along the flight line.

The image acquisition over-flights were conducted in early September, during night-time hours, under clear sky conditions, when colder air temperatures are usually rapidly attained at those altitudes and time of the year, due to irradiative cooling of the surface. Typical night-time image acquisition campaign ranged from 11:30 pm to 3:00 a.m. Though the coldest air temperatures are usually reached just prior to sunrise, we avoided flying at those hours due to the increased amount of water vapor being generated over the hot pools which confound the retrieval of actual surface temperatures.

Thermal infrared images were acquired with a FLIR SC640 camera. The camera is fully digital with non-interlaced images, resulting in crisper, high quality digital images obtained at 30 frames per second. The camera is set to always acquire imagery with the range of -40 to 120 ºC, so over or under saturation of the pixels is always avoided in the case of the typical temperatures observed during the flights in Yellowstone. The images are stored on a computer disk in a digital movie format and later extracted using software at the appropriate overlap and contrast.

Additional flights were conducted during the daytime around 1:00 to 2:00 p.m. local time under clear skies, usually the hottest time of the day, in order to acquire multispectral shortwave imagery and LiDAR imagery. The shortwave band imagery was acquired at 1-meter spatial resolution and used to correct the temperatures obtained from the thermal imagery for surface emissivity. This process will be described in the next section.

LiDAR Data Acquisition

The Utah State U USTAR Center for Active Sensing and Imaging has designed and developed the LASSI (Lidar Assisted Stereo Imager) instrument that is now approved by the FAA to operate on the USU Cessna TP206 remote sensing aircraft.

The LiDAR system uses a full-waveform Riegl Q560 LiDAR transceiver, a Novatel SPAN LN-200 GPS/IMU Navigation System. The LiDAR is capable of working

at up to 1200m above ground level (agl) and, depending on the flying height, at a pulse rate of up to 250,000 shots per second. It has beam divergence of less than 0.5 mrad and therefore has a footprint size of about 0.5 m at 1000 m agl. An average flying height above ground level of 800 m is proposed for the Yellowstone sites which, given a pulse rate of 100,000 shots per second, a flight speed of 180 Km/h and a scan rate of 115 Hz, will yield an average shot density of 5.2 shots per square meter. Given a 50% side-lap specification, an average shot spacing of greater than 5 shots per square meter is anticipated. The waveform for each shot will be digitized at a rate of 500 MHz which yields a volume spacing of 0.6 m for each single shot within the vegetation. Figure 1 shows the LASSI LiDAR system installed in the USU Cessna TP206 remote sensing aircraft.

Originally, only one LiDAR flight was planned for September 2010. The flight on September 9, 2011 also included an area from the 2010 LiDAR Mapping Project near the Mammoth. This area was re-flown in 2011 to compensate for several data holidays, caused by highly varied terrain, that were discovered in the 2010 data during processing.

Color photos Acquired During LiDAR Missions

Color photos were collected by a Cannon EOS 5D Mark II camera at 21.1 megapixels generating .jpg images with a resolution of 5616 (width) x 3744 (height) pixels. Multispectral photos were collected by three Kodak MegaPlus 4.2i cameras. Imagery is initially stored in a binary format.

Figure 2. The LASSI instrument installed in the USU Cessna TP206 remote sensing aircraft.

Image Processing

The individual spectral band images from the shortwave band digital cameras of the USU system are 2012 x 2014 pixels in size, thus at 1-meter pixel resolution, each image covered and area of approximately 2 x 2 Km. The single band images were first corrected for lens vignetting effects (Neale and Crowther, 1994) and for lens radial distortions (Sundararaman and Neale, 1999) and registered into 3-band images ready for geo-rectification. This was accomplished using common control points obtained from a digital color-IR orthophotoquad produced by the Wyoming Geographic Advisory Committee. A 3rd order polynomial transformation was used. The root mean square (rms) error for the individual image rectification was kept to less than one meter. The rectified images were then stitched along the flight lines forming image strips. These strips were calibrated to a reflectance standard using the system calibration obtained through a similar procedure as that described by Neale and Crowther (1994). The incoming irradiance from the sun and sky was measured every minute using an Exotech radiometer with similar spectral bands placed overlooking (from nadir) a standard reflectance panel with known bi-directional properties setup in a central location in the Park (Figure 2). Once the image strips were calibrated, they were stitched together forming a mosaic covering the entire study area.

The calibrated and rectified 3-band mosaic was then used as the base map for rectification of the thermal imagery as it was acquired on the same date and better represented the surface conditions at the time. In addition, it was important that thermal images match the 3-band mosaic as the latter would be used in the correction of the thermal image for surface emissivity.

Each thermal image was rectified using common control points with the 3-band mosaic and then stitched together along the flight lines to form image strips. These were then calibrated using the camera calibration files for the FLIR SC640) to obtain at-aircraft temperatures. Several calibrated strips are then stitched together to form a mosaic covering the study area.

The at-aircraft temperature images were corrected for atmospheric effects at the time of the over flight using the MODTRAN radiative transfer model (Berk et al, 1989). For such, radiosonde data from a nearby weather station (Riverton, WY) was used to obtain the profile of air temperature, dew point temperature and pressure between the surface and the aircraft altitude, required by the model. The profile was adjusted to compensate for the differences in ground surface altitudes. The correction for surface emissivity was based on the technique by Brunsell and Gillies (2002) described below:

The Normalized Difference Vegetation Index (NDVI) was applied to the calibrated 3-band image mosaic obtaining an image layer:

$$NDVI = (NIR - Red) / (NIR + Red) \tag{1}$$

The NDVI was then scaled to obtain the N* parameter in raster form:

$$N^* = (NDVI - NDVI_0)/(NDVI_{max} - NDVI_0) \tag{2}$$

Where $NDVI_0$ is the bare soil NDVI value of the scene and $NDVI_{max}$ is the maximum NDVI of the scene corresponding to full cover dense vegetation.

The fraction of vegetation cover (Fr) becomes:

$$Fr = N^{*2} \qquad\qquad\qquad (3)$$

The surface emissivity layer is obtained by linearly scaling the emissivity between bare soil ($\varepsilon_{soil} = 0.92$) and full dense vegetation cover ($\varepsilon_{veg} = 0.98$) using the Fr image layer:

$$\varepsilon_{surf} = Fr\,(\varepsilon_{veg}) + (1 - Fr)\,\varepsilon_{soil} \qquad\qquad (4)$$

Standing water was taken into account separately. A classification of the 3-band image was conducted to extract a water body mask layer and used in a model within ERDAS Imagine to assign an emissivity of 0.985 to clear water surfaces present in the scene, mostly lakes and hot pools. Finally, the emissivity layer and the at-aircraft temperature image corrected using the MODTRAN model results are used in an ERDAS Imagine model to obtain the at-surface temperature image, corrected for atmospheric effects and surface emissivity. In general, these corrections increased the values of the at-aircraft temperatures by several degrees.

LiDAR Processing

Data Storage

Data collection of the survey area resulted in a total of sixty two (62) flight lines covering the project area. After the mission, all raw navigation data, raw LiDAR data, raw image data, coverage data, and flight logs were offloaded to a computer and an additional backup storage copy created.

Navigation System

Raw GPS/IMU data from the airborne navigation system and raw GPS data from two IGS base stations are processed in Waypoint Inertial Explorer software (www.novatel.com) to produce a solution for aircraft position and attitude. Two IGS base stations were chosen for their proximity to the survey sites, with P711 used for the Lower Geyser Basin and Norris and MAWY used for Mammoth Springs. The coordinates for the two base-stations were calculated specifically for the date of the collection using the online SECTOR tool (http://sopac.ucsd.edu/processing/coordinates/sector.shtml).

These base station coordinates establish a geo-position relative to the WGS84 datum and are valid for the epoch data that was collected from which the navigation solution and subsequent LiDAR points are derived. GPS/IMU data is processed independently forward and backward in time, combined, and smoothed. The difference between forward and reverse solutions is used to assess solution accuracy. At export, the

trajectory data is transformed to the NAD83(CORS96) project datum for use in the LiDAR processing.

LiDAR System

LiDAR waveform files were analyzed using RiAnalyze software to discriminate data points. These points are output in the internal coordinate system of the LiDAR scanner. Each data point is assigned an echo value so it can be used in point classification work. RiProcess then uses the trajectory files created from the raw navigation data to generate XYZ points in a world coordinate system. A boresite calibration and strip (single scan line) adjustment was performed in RiProcess to improve data accuracy. This project's data were processed in strip form, meaning each flight line was processed independently. Processing the lines individually provides the data analyst with the ability to quality control (QC) the overlap between lines. To assess trajectory integrity, individual flight strips were then checked against adjacent strips to ensure good matching in the dataset.

Each flightline (strip) was then brought into Terrascan (by TerraSolid) in the project datum and coordinate system. These flightlines were then combined and several classification routines, customized for the given terrain and vegetation, were then run to classify the points into standard ASPRS/LAS default classifications. Final bare-earth DEMs and DSMs were derived from a Triangulated Irregular Network (TIN) of the classified LiDAR point clouds.

Color and Multispectral Imagery Acquired During LiDAR Missions

Prior to mosaic creation, multispectral raw images were created from the raw imagery acquired by three separate cameras, each with a unique lens filter resulting in three images, taken at the same time – each recording different spectral signatures. Imagery from these cameras is stored in a binary format which is later processed into three (3) separate .tif images representing the individual spectral bands. Vignetting correction is applied, and then the three image bands are combined into a multispectral (false color) image with a resolution of 2068 (width) x 2077 (height) pixels.

Color and Multipsectral Images were then processed by Terraphoto (by TerraSolid). During collection, raw images were stored with a unique timestamp which, used in relation to the flight trajectory and time, provided an initial projected rectification location for each raw image. Mission specific camera calibration parameters were adjusted, and image location was refined to align with neighboring images. Images were projected onto the collected LiDAR points, overlapping portions of the images were cut at automatically generated seamlines. Feathering was applied to the seamlines, and the orthorectified mosaic images were output as .tif images with associated .tfw files organized in a tiling system; each tile representing an area of 1000 m x 1000 m GSD. Pixel size for color ortho-mosaics was set at 16 m resulting in an image with 6250 x 6250 pixel resolution. Similarly, pixel size for multispectral ortho-mosaics was set at .40 m resulting in an image with 2500 x 2500 pixel resolution. The imagery was then checked for quality control purposes and prepared for delivery.

RESULTS AND DISCUSSION

Samples of 2010-2011 delivered products and visualizations

This section presents samples of the delivered visible imagery and derived topography over the 2-year flight period. Refer to the Methods section for information about processing.

The visible imagery acquired during the LIDAR missions allowed the production of a visible, orthorectified base map covering a strip along the Yellowstone River, Gardner River, Park Headquarters and the Mammoth terraces. North of Yellowstone National Park, La Duke Hot Springs (Figure 3) is near the northern limit of the airborne image acquisition. La Duke hot springs occurs within the controlled groundwater area of the Montana Compact. The town of Gardiner, Montana occurs near the junction of the Yellowstone and Gardner rivers (Figure 4). The popular bathing locality of Boiling River occurs along the southern end of the river flight lines (Figure 5). A series of flight lines that intersected the river flight lines covers the Yellowstone National Park Headquarters (Figure 6) and the Mammoth hydrothermal system.

Ground digital elevation models (DEM) derived from the LIDAR acquisition provide a visualization of the various areas along the river corridors and Mammoth Hot Springs. The shaded relief, ground DEM for a portion of Gardiner (Figure 7) clearly shows the incision of the Yellowstone River and the Garner River into the surrounding landscape.

Both the ground DEM and the visible, orthorectified mosaic are reliable base maps for the nighttime thermal infrared acquisitions. The overlay of derived thermal imagery shapefiles (50° to 19^oC) on the shaded relief ground DEM clearly shows the inflow of thermally influenced water into the valley of the Yellowstone River (Figure 8).

Future Work

The new, reliable base maps along the Yellowstone and Gardner rivers as well as the Mammoth hydrothermal system now allows for reliable change detection. We will apply the techniques for calibration and correction of the nighttime thermal infrared imagery developed through the previous collaborative work and can generate reliable, orthorectified maps of estimated heat flow for hydrothermal areas near Mammoth. These base maps are the basis for various applied studies.

Conclusion

This report outlines a new collaboration of the hydrothermal monitoring program. This new collaboration integrates night-time thermal infrared imagery with LiDAR imagery and establishes reliable, orthorectified base maps for change detection within hydrothermal areas.

Figure 3. Portion of orthorectified, visible mosaic covering La Duke Hot Springs. Bright red shows vegetation reflecting near-infrared energy (0.795-0.809 microns).

Figure 4. Portion of orthorectified, visible mosaic covering Gardiner, Montana. Bright red shows vegetation reflecting near-infrared energy (0.795-0.809 microns).
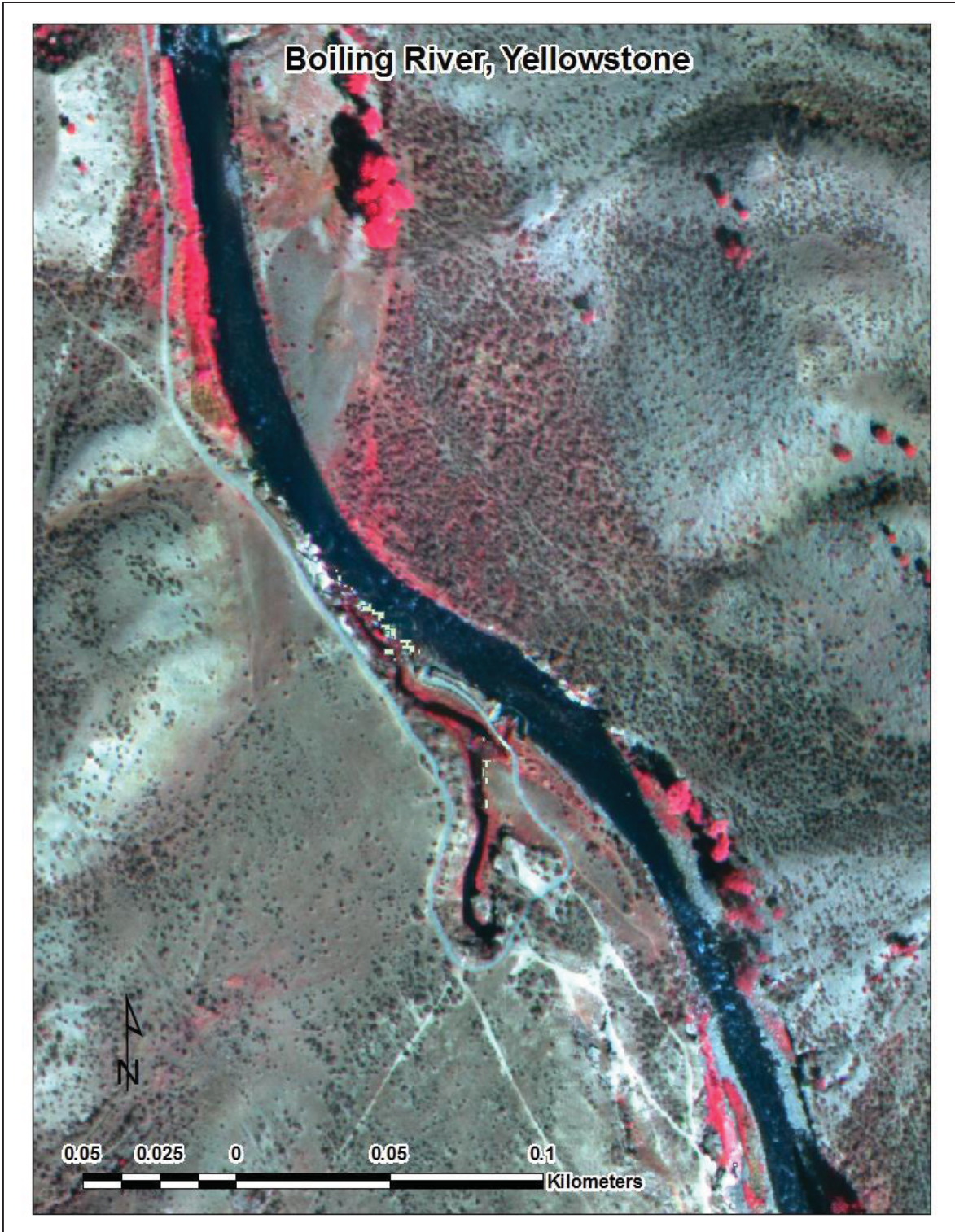
Figure 5. Portion of orthorectified, visible mosaic for Boiling River, Yellowstone National Park. Bright red shows vegetation reflecting near-infrared energy (0.795-0.809 microns).

Figure 6. Portion of orthorectified, visible mosaic for Park Headquarters at Mammoth Hot Springs, Yellowstone National Park. Bright red shows vegetation reflecting near-infrared energy (0.795-0.809 microns).
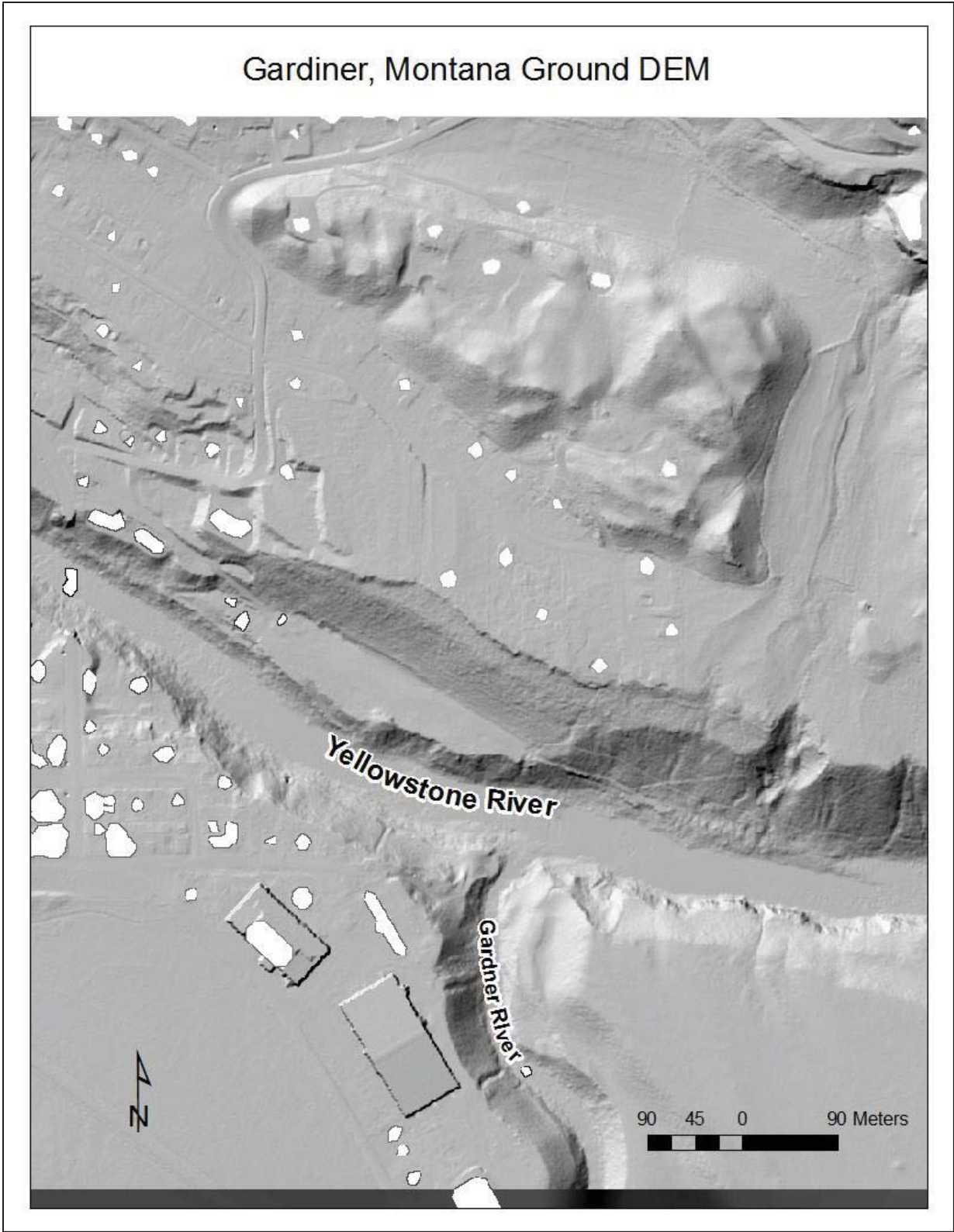
Figure 7. Shaded relief, ground DEM tile showing eastern portion Gardiner Montana and the North Entrance of Yellowstone National Park (bottom-left).
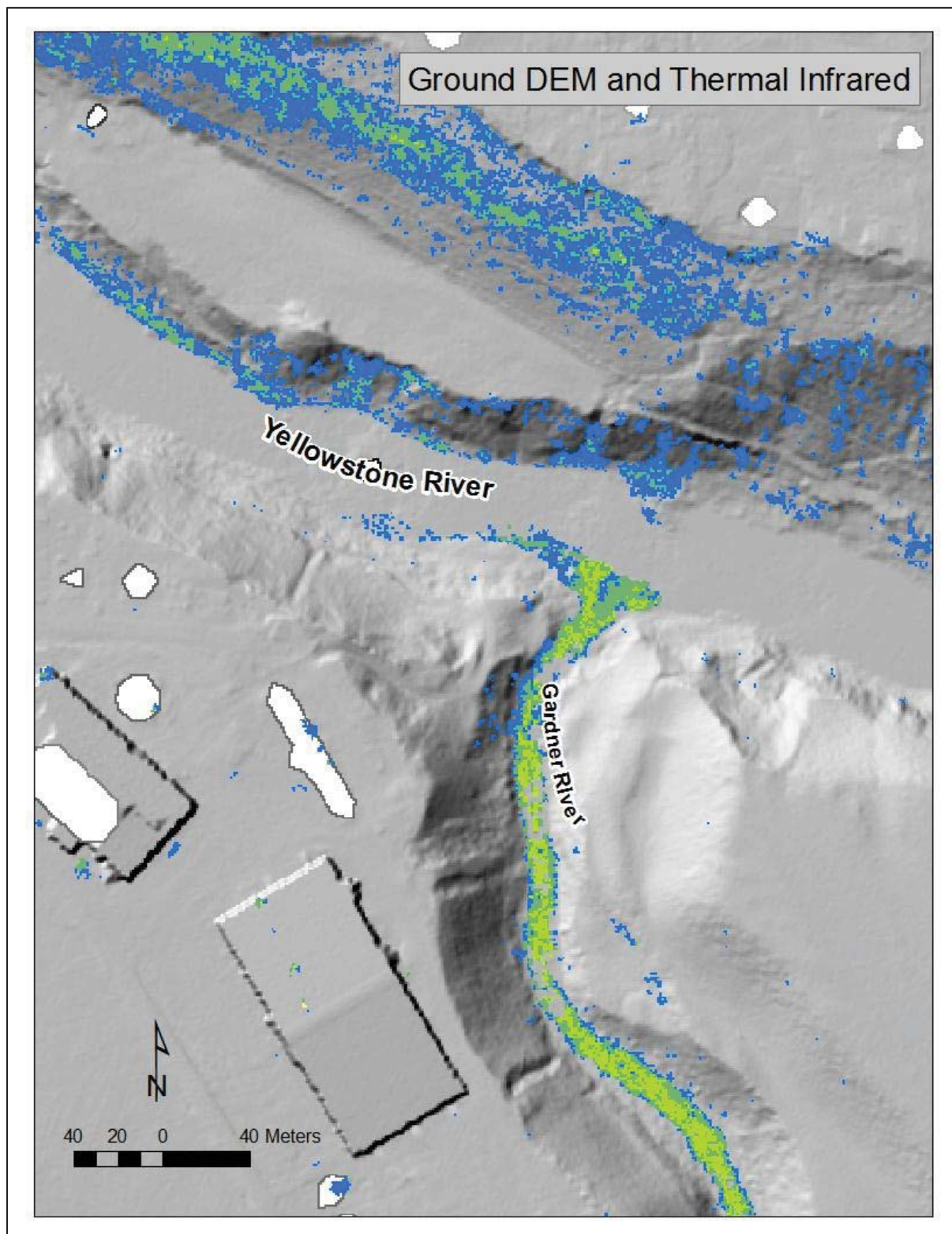
Figure 8. Shaded relief, ground DEM and derived thermal infrared shapefiles (green-19° to 25°C; blue-18° to19^{o}C) for the intersection of the Gardner River with the Yellowstone River.
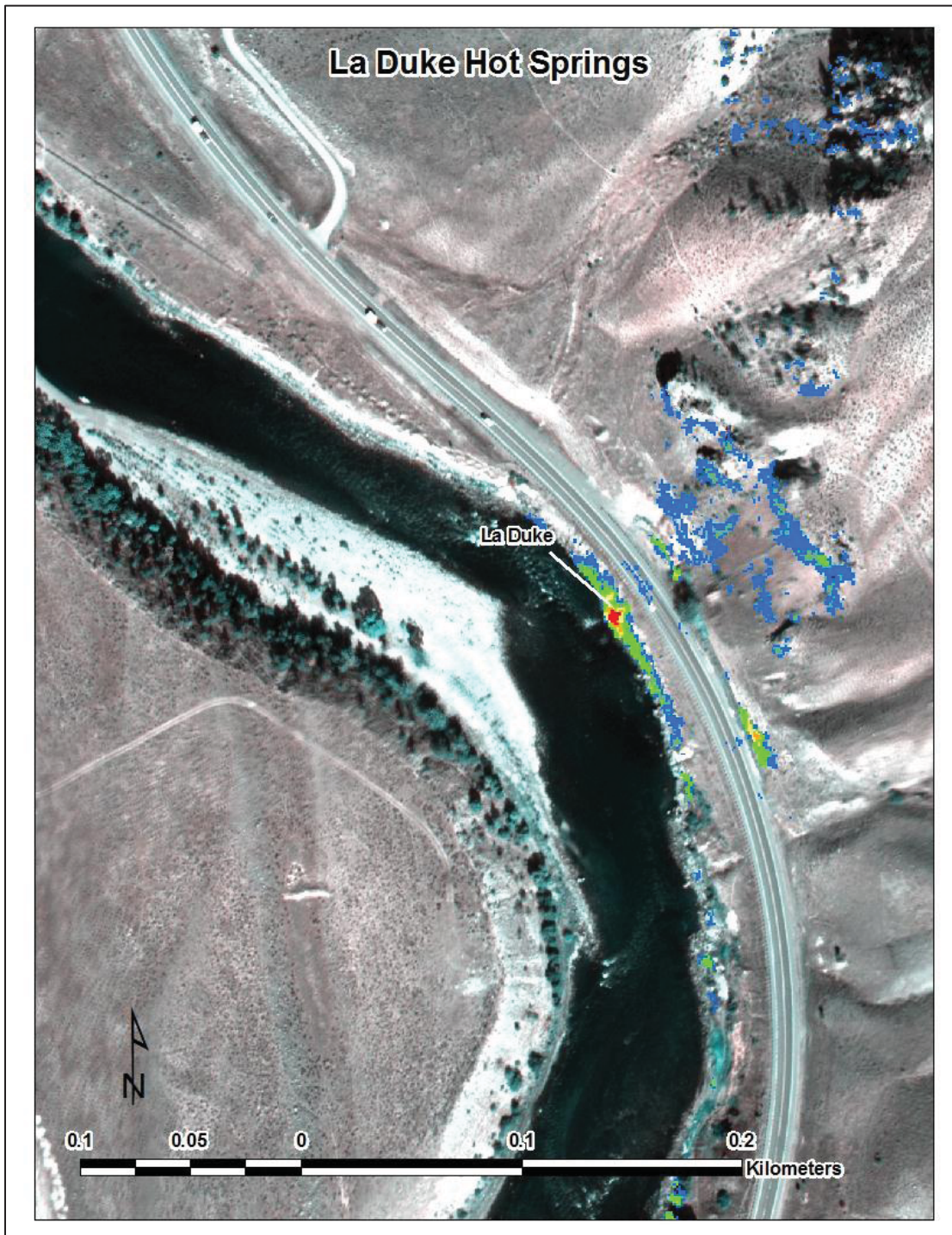
Figure 9. Map showing visible, orthorectified mosaic and night-time TIR for La Duke Hot Springs. Derived thermal infrared shapefiles show various components of the system. Hottest portion is red (40° to 50^oC), orange (30° to 40^oC) and yellow (25° to 30^oC). Coolest portion of the system are green (25° to 19^oC) and blue (18° to 19^oC). Near-infrared vegetation displayed as green in this map.

REFERENCES

Berk, A., Bernstein, L.S., and Robertson, D.C. "MODTRAN: a moderate resolution model for LOWTRAN 7", Report GL-TR-89-0122. Geophysics Laboratory, Bedford, Maryland, USA. (1989)

Brunsell, N.A., and Gillies, R. "Incorporating Surface Emissivity into a Thermal Atmospheric Correction." Photogrammetric Engineering & Remote Sensing. Vol. 68 (12), pp. 1263-1269 (2002)

Cai, B. and Neale, C. M. U., "A Method for Constructing 3-Dimensional Models from Airborne Imagery" In: Color Photography and Videography for Resource Assessment. Proceedings of the 17th Biennial Workshop. American Society for Photogrammetry and Remote Sensing, Bethesda, MD (1999).

Chávez, J. L., Neale, C. M. U., Hipps, Prueger, J. H. and Kustas, W. P., "Comparing aircraft-based remotely sensed energy balance fluxes with eddy covariance tower data using heat flux source area functions." Journal of Hydrometeorology. Vol. 6, No. 6, 923-940 (2005).

Neale, C.M.U, and Crowther, B., "An airborne multispectral video/radiometer remote sensing system: development and calibration.", Remote Sens. Environ. Vol.49 (3), pp.187-194 (1994)

Quattrochi, D.A and J.C. Luvall, [Thermal Remote Sensing in Land Surface Processes], CRC Press, Boca Raton, Florida (2003).

Sundararaman, S. and Neale, C. M. U. , "Geometric Calibration of the USU Videography System", In: Videography and Color Photography for Resource Assessment. Proceedings of the 16th Biennial Workshop. American Society for Photogrammetry and Remote Sensing, Bethesda, MD. (1997)

Torgersen, C.E., Faux, R.N., Mcintosh, B.A., Poage, N.J., and D.J. Norton. "Airborne thermal remote sensing for water temperature assessment in rivers and streams." Remote Sensing of Environment. Vol. 76, 386-398 (2001).